Intelligent Control Algorithms for Robotic-Assisted Beating Heart Surgery

Özkan Bebek, *Student Member, IEEE*, and M. Cenk Çavuşoğlu, *Senior Member, IEEE*

***Abstract*—This paper focuses on the development of control algorithms for intelligent robotic tools that assist off-pump coronary artery bypass graft (CABG) surgery. In the robotic-assisted CABG surgery, the surgeon operates on the beating heart using intelligent robotic instruments. Robotic tools actively cancel the relative motion between the surgical instruments and the point of interest on the beating heart, dynamically stabilizing the heart for the operation. This algorithm is called active relative motion canceling (ARMC). Here, a model-based intelligent ARMC algorithm employing biological signals, such as electrocardiogram, to achieve effective motion cancelation is proposed. Finally, experimental results of the algorithm on a 3-degree-of-freedom robotic test-bed system are reported.**

***Index Terms*—Electrocardiogram (ECG), medical robotics, model predictive control, motion canceling, real-time tracking.**

I. Introduction

ALTHOUGH off-pump coronary artery bypass graft (CABG) surgery is in a nascent stage and only applicable to limited cases, it is preferred over on-pump CABG surgery because of the significant complications resulting from the use of cardio-pulmonary bypass machine, which include long term cognitive loss [1], and increased hospitalization time and cost [2]. On the other hand, off-pump grafting technology is crude and only applicable to a small portion of the cases because of the technological limitations, inadequate for all but the largest diameter target vessels, not effectively applicable to the coronary arteries on the side and the back of the heart, and limited to small number of bypasses. Off-pump procedures represent only 15%–20% of all CABG surgeries, at best [3]. Manual tracking of the complex heartbeat motion can not be achieved by a human without phase and amplitude errors [4]. Use of robotics technology will overcome limitations, as it promises an alternative and superior way of performing off-pump CABG surgery. In this project, it is aimed to develop telerobotic tools to actively track and cancel the relative motion between the surgical instruments and the heart by active relative motion canceling (ARMC) algorithms, which will allow CABG surgeries to be performed on a stabilized view of the beating heart with the technical convenience of on-pump procedures.

This paper explains the design and implementation of intelligent ARMC control algorithms for robotic telesurgical systems, utilizing biological signals in a model-based predictive control fashion. Effective motion canceling in the model-based intelligent ARMC algorithm is achieved by utilizing biological signals, such as electrocardiogram (ECG), in the estimation of the heart motion.

The rest of this section presents the overall system concept and reviews the related work in the literature. In Section II, analysis of the experimental heart motion data, the importance of the ECG signal and the method for ECG wave form detection are discussed. Details on the ARMC algorithm are provided in Section III. Section IV describes the estimation and control algorithms used in the tracking problem. In Section V, simulation and experimental results are given. Finally, the discussion is presented.

A. *System Concept for Robotic Telesurgical System for Off-Pump CABG Surgery*

Robotic-assisted surgery concept replaces conventional surgical tools with robotic instruments which are under direct control of the surgeon through teleoperation, as shown in Fig. 1. The surgeon views the surgical scene on a video display with images provided by a camera mounted on a robotic arm that follows the heart motion, showing a stabilized view. The robotic surgical instruments also track the heart motion, canceling the relative motion between the surgical site on the heart and the surgical instruments. As a result, the surgeon operates on the heart as if it were stationary, while the robotic system actively compensates for the relative motion of the heart. This is in contrast to traditional off-pump CABG surgery where the heart is passively constrained to dampen the beating motion. We call the proposed control algorithm "Active Relative Motion Canceling (ARMC)" to emphasize this difference. Since this method does not rely on passively constraining the heart, it would be possible to operate on the side and back surfaces of the heart as well as the front surface using millimeter scale robotic manipulators that can fit into spaces the surgeon can not reach.

B. *Related Work in the Literature*

Earlier studies in the literature on canceling biological motion in robotic-assisted medical interventions focus on canceling respiratory motion. Sharma *et al.* and Schweikard *et al.* studied the compensation of the breathing motion in order to reduce the

Manuscript received June 10, 2006; revised December 1, 2006. This paper was recommended for publication by Associate Editor L. Whitcomb and Editor F. Park upon the evaluation of the reviewers' comments. This work was supported in part by the National Science Foundation under Grants CISE IIS-0222743, EIA-0329811, and CNS-0423253, and in part by the U.S. Department of Commerce under Grant TOP-39-60-04003. This paper was presented in part at the IEEE International Conference on Advanced Robotics, Seattle, WA, 2005; in part at the IEEE International Conference on Robotics and Automation, Orlando, FL, 2006; and in part at the International Conference of the IEEE Engineering in Medicine and Biology Society, New York, NY, 2006.

The authors are with the Department of Electrical Engineering and Computer Science, Case Western Reserve University, Cleveland, OH 44106 USA (e-mail: ozkan@case.edu; cavusoglu@case.edu).

Color versions of Figs. 1 and 7 are available online at http://ieeexplore.ieee.org.

Digital Object Identifier 10.1109/TRO.2007.895077

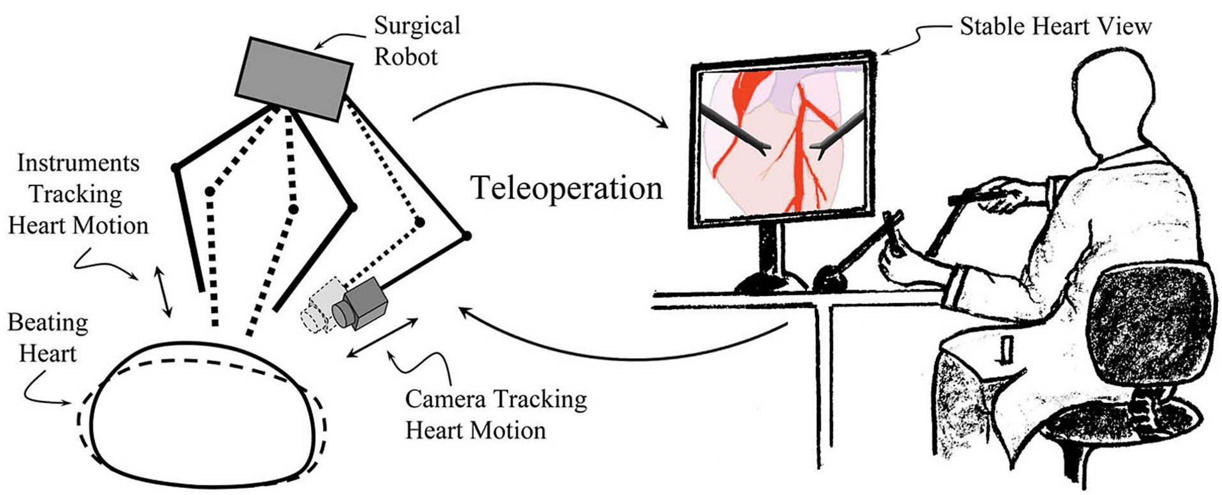

Fig. 1. System concept for robotic telesurgical system for off-pump CABG surgery with ARMC. Left: Surgical instruments and camera mounted on a robot actively tracking heart motion. Right: Surgeon operating on a stabilized view of the heart and teleoperatively controlling robotic surgical instruments to perform the surgery.

applied radiation dose to irradiate tumors [5], [6]. Both studies concluded that motion compensation was achievable. In [7], Riviere *et al.* looked at the cancelation of respiratory motion during percutaneous needle insertion. Their results showed that an adaptive controller was able to model and predict the breathing motion. Trejos *et al.* conducted a feasibility study on the ability to perform tasks on motion-canceled targets, and demonstrated that tasks could be performed better using motion canceling [8].

Madhani and Salisbury [9] developed a 6-degree-of-freedom (DOF) telesurgical robot design for general minimally invasive surgery, which was later adapted by Intuitive Surgical Inc., Palo Alto, CA, for their commercial system, called daVinci. Computer Motion Inc., Goleta, CA (Computer Motion Inc. was acquired by Intuitive Surgical Inc., and does not exist anymore), developed a 5-DOF telesurgical robotic system, called Zeus, with scaled motions for microsurgery and cardiac surgery. Both of these systems are currently in use for cardiothoracic surgery applications. These systems are designed to enable dexterous minimally invasive cardiac surgery, and they are neither intended nor suitable for off-pump CABG surgery with ARMC, because of their size, bandwidth, and lack of motion tracking capabilities. These systems can only perform on-pump or off-pump CABG surgery by using passive stabilizers, and, therefore, have the same limitations as conventional tools described above.

In [10], Nakamura *et al.* performed experiments to track the heart motion with a 4-DOF robot using a vision system to measure heart motion. The tracking error due to the camera feedback system was relatively large (error on the order of few millimeters in the normal direction) to perform beating heart surgery. There are also other studies in the literature on measuring heart motion. Thakor *et al.* used a laser range finder system to measure 1-D motion of a rat's heart [11]. Groeger *et al.* used a two-camera computer vision system to measure local motion of heart and performed analysis of measured trajectories [12], and Koransky *et al.* studied the stabilization of coronary artery motion afforded by passive cardiac stabilizers using 3-D digital sonomicrometry [13].

In [14] and [15], Ortmaier *et al.* used an ECG signal in the visual measurement of heart motion using a camera system, for estimation of the motion when the surgical tools occluded the view. They reported significant correlations between heart surface trajectory and ECG signals, which implies these inputs can be used interchangeably. Therefore, these two independent components were considered as inputs to the estimation algorithm. In their study, heart motion estimation was not based on a heart motion model and it was completely dependent on previously recorded position data. Actual tracking of the heart motion using a robotic system was planned as a future work.

More recently, in a pair of independent parallel studies by Ginhoux *et al.* [16] and Rotella [17], motion canceling through prediction of future heart motion was demonstrated. In both studies, model predictive controllers were used to get higher precision tracking. In the former, a high-speed camera was used to measure heart motion. Their results indicated a tracking error variance on the order of 6–7 pixels (approximately 1.5–1.75 mm calculated from the 40 pixel/cm resolution reported in [16]) in each direction of a 3-DOF tracking task. Although it yielded better results than earlier studies using vision systems, the error was still very large to perform heart surgery, as operation targets to be manipulated using the robotic systems in a CABG surgery are blood vessels with 2 mm or less diameter. In [17], by a 1-DOF test bed system accuracy very close to the desired error specifications for heart surgery was achieved, and Rotella concluded that there still was a need for better prediction of heart motion.

A heart model was proposed by Cuvillon *et al.* in [18], based on the extraction of the respiration motion from the heartbeat motion using the QRS wave form of the ECG and lung airflow information as sensory inputs. They concluded that heartbeat motion is not the product of two independent components, in fact the heartbeat motion is modulated by the lung volume.

II. Analysis of Heart Data

In this section of the paper, the experimentally collected heart motion data used in this study are described. The data were collected from an animal model (an adult porcine), and all study was done with this prerecorded data. Here, first the collection of heart motion data will be explained. The requirements for the tracking will be calculated in the data analysis section. Next, ECG, the biological signal employed, and its use in this research will be explained. Last, a short description of the real-time ECG wave form detection will be given.

A. Experimental Setup for Measurement of Heart Motion

A sonomicrometry system manufactured by Sonometrics, Inc. (London, ON, Canada) was used to collect the heart motion data used in this study. A sonomicrometer measures the distances within the soft tissue via ultrasound signals. A set of small piezoelectric crystals embedded, sutured, or otherwise fixed to the tissue are used to transmit and receive short pulses of ultrasound signal, and the "time of flight" of the sound wave as it travels between the transmitting and receiving crystals are measured. Using these data, the 3-D configuration of all the crystals can be calculated [19]. No analog conversion process is involved in these measurements, which eliminates the need to calibrate the system. Crystal operation frequency of 64 MHz provides resolution of 24 μm in the measurement of intertransducer distances [20]. Absolute accuracy of the sonomicrometry system is 250 μm (approximately $1/4$ wavelength of the ultrasound) [21].

The sonomicrometry system has an important advantage over using a vision system, which is the sensor of choice in the earlier works in the literature, for measuring heart motion for robotic ARMC. A stand-alone vision system is not suitable for use during surgical manipulation because the surgical instruments (including the robotic tools) will occlude the point of interest (POI) rendering the vision system practically useless, whereas the sonomicrometry system does not have this shortcoming. Although an algorithm was developed by Ortmaier in [14] to estimate the heart motion, when the view is occluded, it is only applicable to brief occlusions.

In the experimental setup, one crystal of the sonomicrometric system was sutured next to the left anterior descending artery (LAD) located on the front surface of the left ventricle of the animal heart, at a point one third of the way from the starting point of the LAD. Six other crystals were asymmetrically mounted on a rigid plastic base of diameter 56 mm, on a circle of diameter 50 mm, forming a reference coordinate frame. This rigid plastic sensor base was inserted behind the heart, inside the pericardial sac, and the motion of the POI on the LAD was measured relative to this coordinate frame. The pericardial sac had been filled with a saline solution, completely immersing the sensor base, which enabled the continuous contact of sonomicrometric sensor system with the heart and proper operation. Data were processed offline using the proprietary software provided with the system to calculate the 3-D motion of the POI. The only filtering performed on the data produced by the sonomicrometry system was the (very limited) removal of the outliers, which occasionally occur as a result of ultrasound echoing effects. Although the sonomicrometry system can operate at 2-kHz sampling rate for measuring the location of the POI crystal relative to the fixed base, in our test experiments, we have collected data at a sampling rate of 257-Hz collecting redundant measurements.

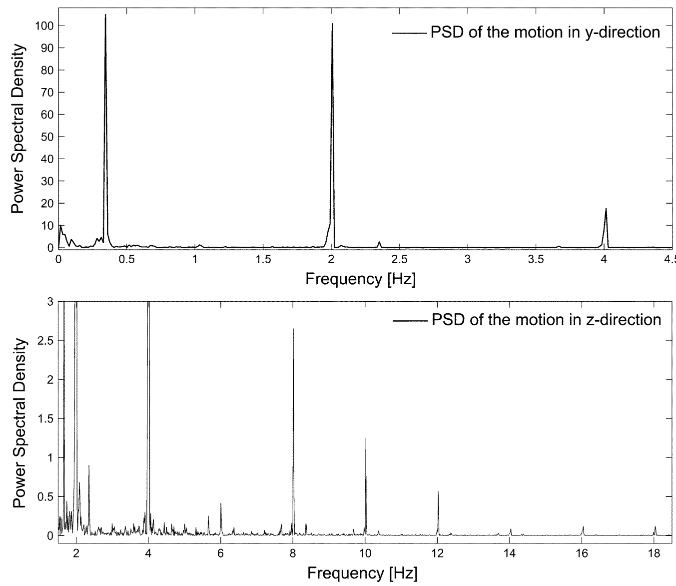

Fig. 2. PSD of the motion of the POI is shown in two different scales. Observable dominant modes are at 0.37 and 2.0 Hz, which correspond to breathing and heartbeat motions, respectively. Peak at the 4.0 Hz is the first harmonic of the heartbeat motion.

B. Analysis of Heart Motion Data

During the 60-s data collection period, the average heart rate of the animal model was 120 beats per minute, as calculated from the ECG signal recorded simultaneously with the motion data. The peak displacement of the POI from its mean location was 12.1 mm, with a root-mean-square (RMS) value of 5.1 mm. Fig. 2 shows the power spectral density (PSD) of the motion of the POI in the y- and z-directions at different scales.

Two observable dominant modes of motion are visible in Fig. 2. The first mode is at 0.37 Hz, which corresponds to the breathing motion. The second dominant mode is at 2.0 Hz which corresponds to the main mode of motion due to heart beating, as it matches the frequency observed from the ECG signal. The peak at the 4.0 Hz is the first harmonic of the heartbeat motion. The component of motion corresponding to breathing motion, which is estimated by filtering the motion data using a lowpass Equiripple FIR filter of cutoff frequency 1.0 Hz, has a RMS magnitude of 2.86 mm. The remainder of motion, which is due to the beating of the heart, has a RMS magnitude of 4.18 mm. The POI motion can be approximated with an error less than 140-μm RMS with frequency components up to 26 Hz. This gives the specifications for the robotic mechanism and ARMC control algorithm design. These results are consistent with the heart motion measurements reported by Groeger in [12]. The data in that study were collected using a stereo vision system. The results of our study confirm the reported results by an experimental setup using an alternate sensory modality, i.e., the sonomicrometry system.

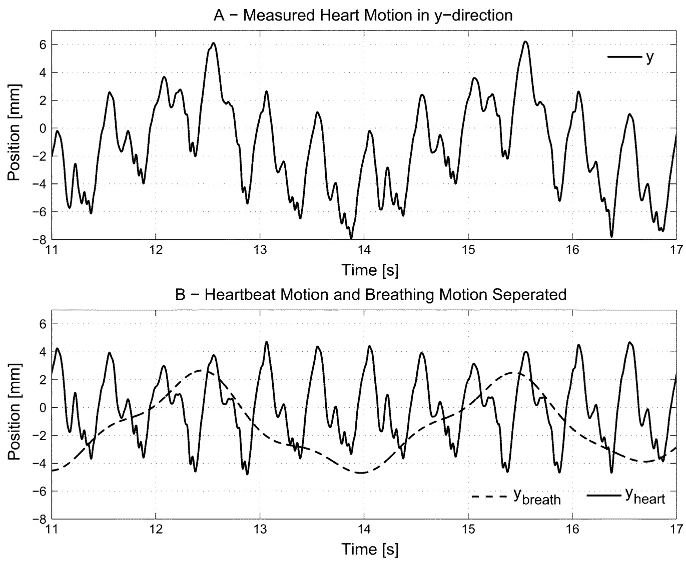

Fig. 3. Separation of breathing motion and heartbeat motion using a low-pass filter with cutoff frequency 1.0 Hz. (A) Motion of the measured POI on the heart in the y-direction. (B) Heartbeat motion and breathing motion separated using a low-pass filter.

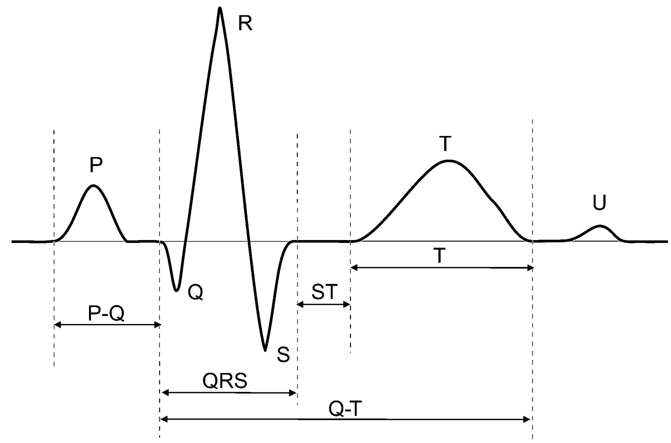

Fig. 4. Typical scalar ECG, showing significant intervals and deflections.

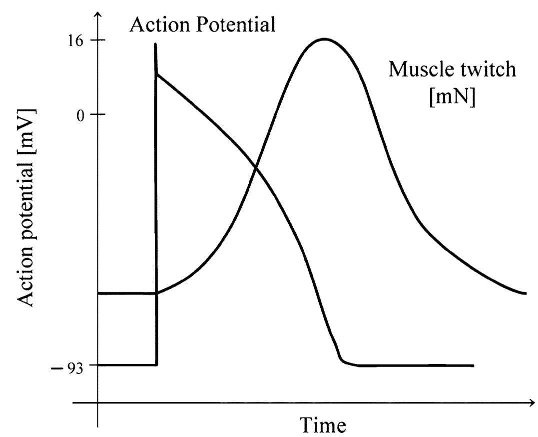

Fig. 5. Time relationship between action potential and mechanical force developed by ventricular muscle. Rapid depolarization of a cardiac muscle fiber is followed by force development in the muscle. The lag between the excitation and the peak force is about 200 ms long.

The control algorithm proposed (detailed in Section III-B) is based on the premise that the heart motion is quasiperiodic and the motion during the previous beats can be used, to some extent, as a feedforward signal during the control of the robotic tool for ARMC. Here, our main concern is with the moderate-to-high frequency components of the motion since they are the most demanding for the mechanism and the ARMC control algorithm. As described above, the low-frequency components of motion typically result from breathing (bandwidth of 1.0 Hz, including the main mode of the breathing frequency) and can easily be canceled using a feedback controller. The feedforward controller is needed to cancel the high frequency components of motion. After the breathing motion is filtered out, the PSD of the motion signal is composed of very narrow peaks at the harmonics of the heartbeat frequency (Fig. 3). This shows that the moderate-to-high frequency component of the motion is quasiperiodic, with frequency equal to heartbeat rate, supporting the feasibility of the ARMC algorithm.

C. ECG as the Biological Signal

The human body acts as a giant conductor of electrical currents. Connecting electrical "leads" to any two points on the body may be used to register an ECG. Thus, ECG contains records for the electrical activity of the heart. The ECG of heart forms a series of waves and complexes that have been labeled in alphabetical order, the P wave, the QRS complex, the T wave and the U wave (Fig. 4) [22]. Depolarization of the atria produces the P wave; depolarization of the ventricles produces the QRS complex; and repolarization of the ventricles causes the T wave. The significance of the U wave is uncertain [23]. Each of these electrical stimulations results in a mechanical muscle twitch. This is called the electrical excitation-mechanical contraction coupling of the heart. Thus, the identification of such waves and complexes can help determine the timing of the heart muscle contractions. Using ECG in the control algorithm can improve the performance of the position estimation because these wave forms are results of physiological processes that causally precede the heart motion and also because ECG is significantly correlated with heartbeat motion [15]. The time relationship between action potential and mechanical force developed by ventricular muscle is shown in Fig. 5 [24], [25]. Rapid depolarization of a cardiac muscle fiber is followed by force development in the muscle. The completion of repolarization coincides approximately with the peak force, and the duration of contraction parallels the duration of the action potential, which is about 150 to 200 ms long. The lag between these two formations enables the prediction of future heart activity. Although this time lag is about 200 ms, it is sufficient for real-time detection of the waves and complexes of the ECG. Average detection time for the test data was 174 ms (see Section II-D for test database details).

The ECG signal employed in this research was collected with the analog data acquisition part of the sonomicrometry system used. The ECG data were recorded simultaneously with the collection of the heart motion data at the same sampling rate of 257 Hz.

D. ECG Wave Form Detection

There is a substantial literature on detecting the ECG characteristic points with high detection accuracies (e.g., [26]–[29]). However, most of these algorithms are designed for offline processing of ECG signals and only a few of them are for real-time detection of ECG signal complexes [30], [31]. The difficulty in detection arises from the diversity of complex wave forms and the noise and artifacts accompanying the ECG signals. In this work, the significant ECG wave forms and points, such as P, QRS, and T, were detected in hard real time[1] by an algorithm adapted from [31]. This one was selected among other available algorithms because it employs signal localization both in time and frequency using wavelet analysis, characterization of the local regularity of the signal and separation of the ECG waves from serious noise, artifacts, and baseline drifts in real time.

A short description of the ECG wave form detection algorithm, included here to make the paper self contained, is as follows. Wavelet transform of the ECG data at the sampling frequency was calculated at scales $2^j, j = 1 \ldots 5$. These energy levels cover the power spectra of ECG signal. The energy of the QRS complex is typically placed in the levels 2^3 and 2^4. The energies of P and T waves are located at levels 2^4 and 2^5. To detect peaks, threshold filters and decision making rules were used in every energy level. First, QRS complexes were detected by locating any peak pairs on the wavelet transforms. Since both QRS and T peak pairs can appear on the same energy levels, unmarked peaks on levels 2^4 and 2^5 were marked as T waves after the possible QRS complexes were identified. P wave detection was done similarly by detecting peak pairs at the energy scale 2^4 which corresponded to neither a QRS complex nor a T wave.

Bahoura *et al.* evaluated the original algorithm in real time with the MIT-BIH Arrythmia Database [32]. This database contains 48 half-hour excerpts of two-channel ambulatory ECG recordings. They reported a 0.26% false detection rate (126 false positive beats and 180 false negative beats out of 116 137 beats), showing the algorithms capability in detecting QRS complexes. We used constant detection parameters instead of adaptive ones, and obtained a 1.49% false detection rate using the same database (408 false positive beats and 709 false negative beats out of 75 010 healthy beats).

With this method, QRS-T-P waves were detected in real time for the collected 56-s ECG data with 100% QRS complex and T wave detection rates, and 97.3% P wave detection rate (Fig. 6). Missed waves were decided according to the ECG state transitions shown in Fig. 8. Detected signals were used to estimate the reference signal as described in Section IV (Fig. 11).

III. Model-Based Active Relative Motion Cancelation

A. Motivation and Methodology

The control algorithm is the core of the robotic tools for tracking heart motion during CABG surgery. The tools need to track and manipulate a fast moving target with very high precision. During free beating, individual points on the heart move as much as 7–10 mm. Although the dominant mode of heart motion is on the order of 1–2 Hz, if we look at measured motion of individual points on the heart during normal beating, there is significant energy at frequencies up to 26 Hz. The coronary arteries that are operated on during CABG surgery range from 2 mm in diameter down to smaller than 0.5 mm, which means the system needs to have a tracking precision in the order of 100 μm. This corresponds to a less than 1% dynamic tracking error up to a bandwidth of about 20 to 30 Hz.

[1]In hard real time, no corrections are allowed to be performed to the past data after the operation deadline expires.

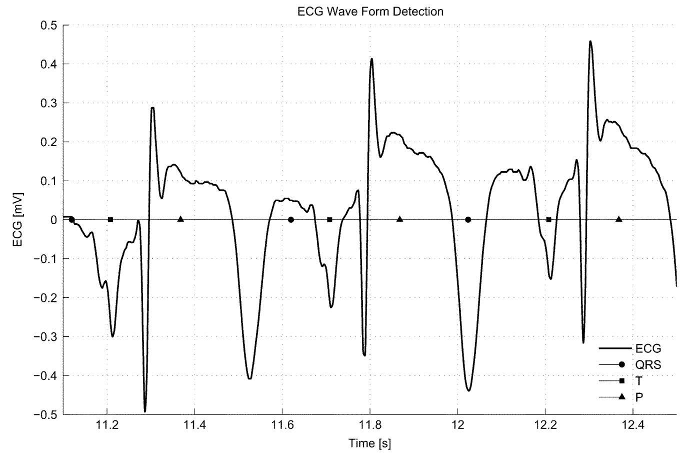

Fig. 6. Detection of ECG wave forms. ●: Detected QRS complex. ■: Detected T wave. ▲: Detected P wave. Note that the marked times correspond to when features are detected, which is delayed from the actual temporal location of the waveform about 170 ms due to the time taken by the detection algorithm.

The specifications for tracking heart motion are very demanding. These stringent requirements could not be achieved using traditional algorithms in earlier attempts reported in the literature [10], [11]. Traditional algorithms rely purely on feedback signal from measurement of heart motion using external sensors, and they do not use any physiological model of the heart motion.

Using a basic model of heart motion can significantly improve tracking performance since heart motion is quasiperiodic [16]. It is also possible to use the information from the biological signals, such as ECG activity, and aortic, atrial, and ventricular blood pressures, to control the robotic tools tracking the heart motion.

The control architecture we are proposing in this research is shown in Fig. 7. In this architecture, the control algorithm utilizes the biological signals in a model-based predictive control fashion. Using biological signals in the control algorithm improves the performance of the system since these signals are results of physiological processes which causally precede the heart motion. A heart motion model can be formed by combining motion data and biological signal data.

In this paper, the ECG signal is used in the heart model. ECG contains records for the electrical activity of the heart. Electrical signals, which stimulate the contraction of the heart muscles, precede the actual contraction by about 150–200 ms, and these signals can be observed in the ECG measurements. Because of this, ECG signal is very suitable for period-to-period synchronization with sufficient lead time for feedforward control, and identification of arrhythmias.

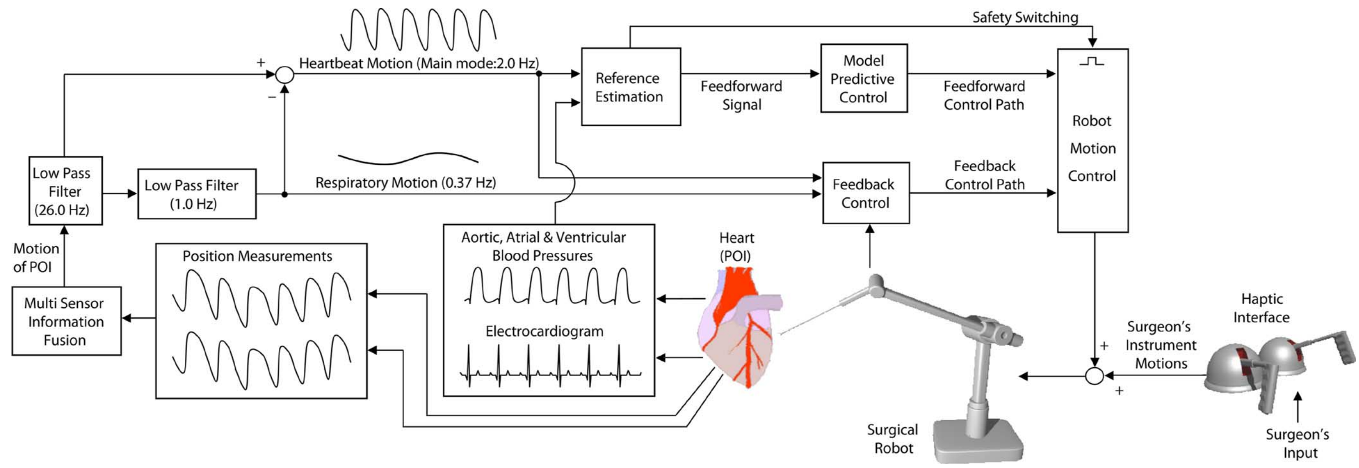

Fig. 7. Proposed control architecture for designing intelligent control algorithms for ARMC on the beating heart surgery.

B. Intelligent Control Algorithms for Model-Based ARMC

In the model-based ARMC algorithm architecture, shown in Fig. 7, the control algorithm uses information from multiple sources: mechanical motion sensors which measure the heart motion, and sensors measuring biological signals. The control algorithm identifies the salient features of the biological signals and uses this information to predict the feedforward reference signal.

The control algorithm also handles the changes in the heart motion, including adapting to slow variations in heart rhythm during the course of the surgery, as well as handling occasional arrhythmias which may have natural causes or may be due to the manipulation of the heart during surgery.

The two dominant modes of the motion of POI are separated by using a pair of complementary filters (Section II-B). The control path for tracking of the heartbeat component of the motion has significantly more demanding requirements in terms of the bandwidth of the motion that needs to be tracked. That is why a more sophisticated feedforward algorithm is employed for this part. Respiratory motion has significantly lower frequency, and it is canceled by a purely feedback based controller. In the proposed architecture (Fig. 7), the robot motion control signal is computed by combining these two parts. The feedforward part is calculated with the signal provided by the heart motion model and the feedback signal is calculated with the direct measurements of heartbeat and respiratory motions. The feedforward controller was designed using the model predictive control [33] and optimal control [34], [35] methodology of modern control theory, as described in Section IV.

The confidence level reported by the heart motion model is used as a safety switching signal to turn off the feedforward component of the controller if an arrhythmia is detected, and switch to a further fail-safe mode if necessary. This confidence level will also be used to adaptively weigh the amount of feedforward and feedback components used in the final control signal. These safety features will be an important component of the final system. Therefore, the best design strategies for developing feedforward motion control was aimed.

In Fig. 8, a finite-state model for the cardiac cycle is shown. The model involves primary states of the heart's physiological

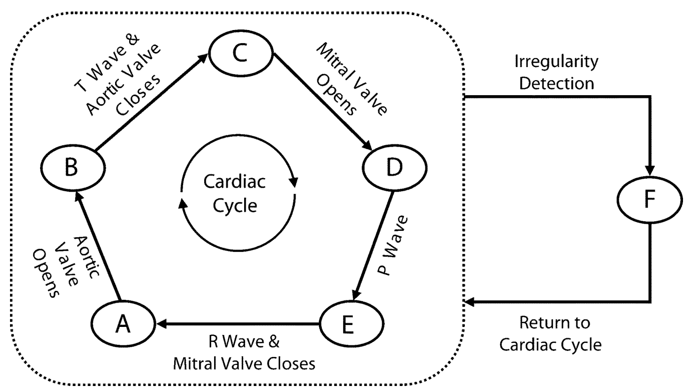

Fig. 8. State model of the beating heart. Transition between the states are depicted using ECG waves and the motion of the heart valves, which can be inferred from blood pressure measurements. States forming the cardiac cycle are: (A) isovolumic contraction; (B) ejection; (C) isovolumic relaxation; (D) ventricular filling; (E) atrial systole; (F) irregularity in the cardiac cycle.

activity. Transitions between the states are depicted using the states of the mitral and aortic valves of heart and P, R, and T waves of the ECG. During the ECG wave form detection process, QRS complex is detected and used in substitute to R wave. Any out of sequence or abnormal states in the cycle can be identified as irregularity. Using this model, rhythm abnormalities and arrhythmias can be spotted and system can be switched to a safer mode of operation.

Although some of the system concepts in the literature are similar to this scheme at the most basic level, there are significant differences including the lack of intelligent model-based predictive control using biological signals, and multisensor fusion with complementary and redundant sensors, which form the core of our proposed architecture. The system by Nakamura *et al.* [10] used purely position feedback obtained from a two-camera computer vision system. Neither biological signals were used in the system, nor was a feedforward control component present. The system by Ginhoux *et al.* [16] utilized a feedforward control algorithm, based on model predictive control and adaptive observers; however, it did not utilize any biological signals. Ortmaier *et al.* [15] utilized ECG using a "model free" method, i.e., without using a heart model in the process.

With the architecture proposed in this paper, the degree of awareness is increased by utilizing a heart motion model in reference signal estimation. Inclusion of biological signals in a model-based predictive control algorithm increases the estimation quality, and such a scheme provides better safety with more precise detection of anomalies and switching to a safer mode of tracking.

IV. Control Algorithms

The control algorithm is the core of the robotic tools for tracking heart motion during CABG surgery. The robotic tools should have high precision to satisfy the tracking requirements [more than 97% motion cancelation (details in Section II-B)]. During free beating, individual points on the heart move as much as 10 mm. Although the dominant mode of heart motion is on the order of 1–2 Hz, if we look at measured motion of individual points on the heart during normal beating, there is significant energy at frequencies up to 20 Hz.

As mentioned earlier, the heart motion is quasiperiodic and previous beats can be used as a feedforward signal during the control of the robotic tool for ARMC. In [17], a model-based predictive controller, which used the estimation of the heart motion, and feedback based controllers were compared on a 1-DOF robotic test-bed system. The model-based predictive controller outperformed the feedback based controllers both in terms of the RMS error and in terms of the control action used. In this paper, we will exclusively focus on model-based predictive controllers.

A key component of the ARMC algorithm, when a predictive controller is used, is estimation of the reference motion of the heart which is provided to the feedforward path. If the feedforward controller has high enough precision to perform the necessary tracking, then the tracking problem can be reduced to predicting the estimated reference signal effectively.

Ginhoux *et al.* [16] used an adaptive observer, which identifies the Fourier components of the past motion at the base heart rate frequency and its several harmonics to estimate the future motion. This approach assumes that the heartbeat rate stays constant. Ortmaier *et al.* [15] estimated the heart motion by matching the current heart position and ECG signals of sufficient length with recorded past signals, assuming that, with similar inputs, the heart would create outputs similar to the ones detected in the past.

In the next two sections (Sections IV-A and IV-B), reference signal estimation schemes used for the ARMC algorithm are described. Then the control problem and its solution are given in Section IV-C.

A. Reference Signal Estimation

A simple prediction scheme that assumes constant heartbeat rate can be used for reference signal estimation. Heartbeat is a quasiperiodic motion with small variations in every beating cycle. If the past heartbeat motion cycle is known, it can be used as an estimate reference signal for the next cycle. Any measured heart position value can be approximated forward one cycle as long as the heartbeat period for that cycle is known. In this case, a constant heartbeat period (0.5 s) was used to store one period length of the heartbeat signal. The motion of the heart from the previous cycle was used as a prediction of the next cycle (Fig. 9). The stored beating cycle was used as the approximate future reference beating signal in the ARMC algorithm.

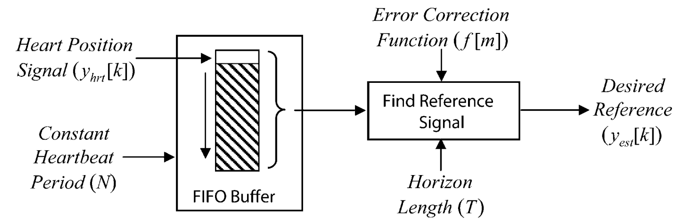

Fig. 9. Reference signal estimation block diagram: Buffered *past heart position data* were used for estimation with approximated constant heartbeat period.

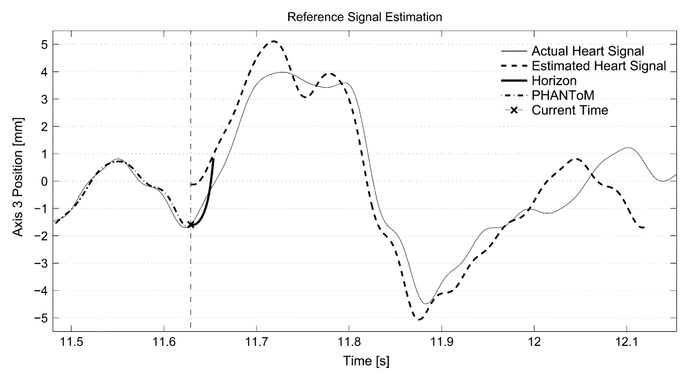

Fig. 10. Reference signal estimation during control action. Observe the horizon signal where the offset between the current position and estimated signal is added gradually starting from current time to horizon steps ahead.

Using the last heartbeat cycle exactly as the future reference would result in large errors due to the quasiperiodic characteristics of the heart motion and other irregularities of the signal. Therefore, instead of using the past beating cycle directly, reference signal was processed online.

Any position offset between starting point of the past cycle, $y_{\mathrm{hrt,pr}}$, and starting point the next cycle (i.e., current position in time), y_{hrt}, were lined up by subtracting the difference, y_{err} (1). However, the added offset was gradually decreased over a constant length of time (hereafter, this length will be referred to as *horizon*, T) using a high-order error correction function defined by (2). This calculation was carried out T steps ahead (3). So, only some percentage of the current error was added to the future signals, and no error was added to the signals T steps ahead (Fig. 10). This maintained the continuity of the signal estimate and converges it onto the actual signal within the horizon ahead

$$y_{\mathrm{err}}[k] = y_{\mathrm{hrt}}[k] - y_{\mathrm{hrt,pr}}[k] \tag{1}$$

$$f[m] = 1 - \left(\frac{m}{T}\right)^p \tag{2}$$

$$y_{\mathrm{est}}[k+m] = y_{\mathrm{hrt,pr}}[k+m] + f(m)\, y_{\mathrm{err}}[k] \quad (m = 0, 1, \ldots, T) \tag{3}$$

where y_{hrt} is the measured motion of the POI on the heart, $y_{\mathrm{hrt,pr}}$ is the measured motion of the previous cycle ($y_{\mathrm{hrt,pr}}[k] = y_{\mathrm{hrt}}[k-N]$, with N being the heartbeat period), y_{est} is the desired reference estimate, k is the current time step, m is the number of steps ahead that the signal is calculated, p is the order of the error correction function, and $f[m]$ is the

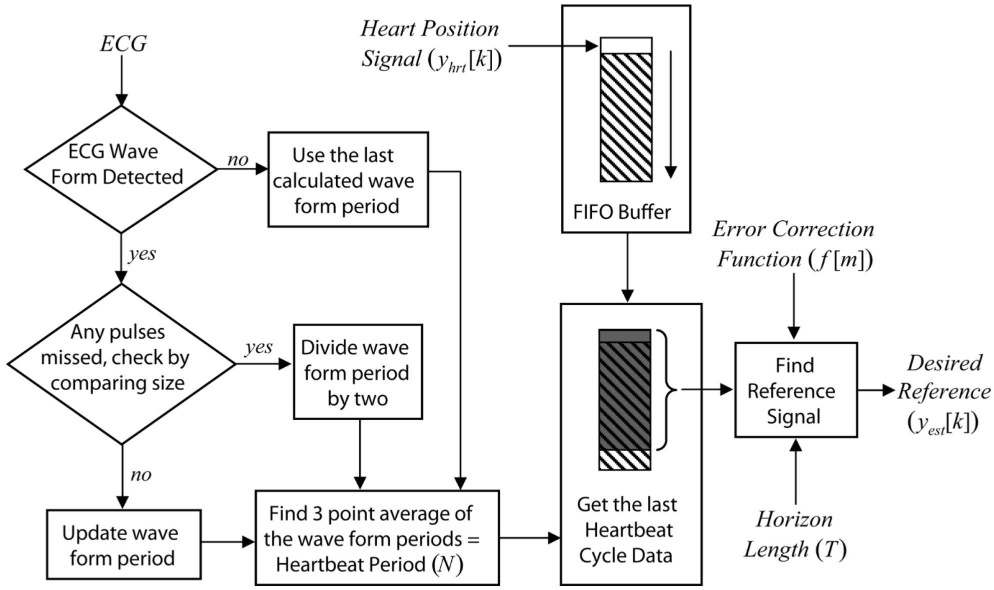

Fig. 11. Simplified finite state model of the reference signal estimation using ECG algorithm. Detected ECG Wave forms were used in the estimation of *reference*, with the buffered *past heart position data*.

polynomial weighting function used. In Fig. 10, the actual and the estimated motions can be seen as the control executes.

B. Reference Signal Estimation Using Biological Signals

Although the position offset between the previous and current beating cycles can be eliminated gradually using the technique above, the error due to changes in heartbeat period remains. Because heartbeat is a quasiperiodic motion with small period variations in every beating cycle, these period changes could result in large offsets in the estimated signal, and can cause jumps during the tracking.

As mentioned earlier in the Section II-C, ECG signal is very suitable for period-to-period synchronization. In this reference signal estimation scheme, rather than using a constant heartbeat period, a variable period calculated using ECG was used. QRS, P, and T waves were used as check points for detecting heartbeat period. In Fig. 11, the block diagram for reference signal estimation using ECG is illustrated.

Here, past heart position data were stored on the fly into a FIFO buffer which was 1300 elements long (650 ms of data, and note that average heartbeat period is about 500 ms long). The most recently stored part of the heart position buffer, in the length of updated heartbeat period using ECG, was used in the estimation.

The current heartbeat period was calculated by averaging the periods of the three ECG wave forms. The period was updated continuously as new wave forms were detected. If detection of any ECG wave form was missed, the period of the missed signal was doubled to compensate for the missing signal. Some upper and lower period boundaries were imposed in order to eliminate any misses by the detection algorithm.

In Fig. 12, the estimated signals just before and after the detection of a new wave form are shown. In Fig. 12(B), observe that after the T wave was detected, the past heartbeat period time mark was shifted back in time as a result of the increase in the heartbeat period. In the example shown with Fig. 12(A) and (B), RMS estimation error for one heartbeat period ahead decreased from 0.887 to 0.456 mm after the shift. With the use of ECG in ARMC algorithm, heartbeat period in the estimation of reference signal can be adjusted online.

C. Receding Horizon Model Predictive Control

Having the estimated trajectory of the next cycle in hand, the following control problem arises: Tracking of heart motion where there is some knowledge of the future motion. Then, this optimal tracking problem can be stated as follows.

Suppose the dynamics of the robotic surgical manipulator is given by an n-dimensional linear system having state equations

$$x[k+1] = \mathbf{\Phi} x[k] + \mathbf{\Gamma} u[k] \tag{4}$$

$$y[k] = \mathbf{H} x[k]. \tag{5}$$

Here, if the dimensions of $\mathbf{\Phi}$, $\mathbf{\Gamma}$, and $\mathbf{H}$ are $n\times n, n\times m$ and $l\times n$, respectively; then, the n-vector $x[k]$ denotes the system state at time k where $x[k_0]$ is given for some time k_0 such that the $k_0 \leq k; m$-vector $u[k]$ denotes system control at time k; and the l-vector $y[k]$ denotes the system output at time k where r entries of y are linearly independent or, equivalently, the matrix $\mathbf{H}$ has rank r. Suppose we are also given an r-vector $y_{\text{est}}[k]$ for all k in the range $k_0 \leq k \leq k_0 + T$ for some times k_0 and T. The optimal tracking problem is then to find the optimal control u for the system (4)–(5), such that the output y tracks the signal y_{est}, minimizing the index (6)

$$J[k] = \sum_{k=k_0}^{k_0+T} \Big((x[k] - x_{\text{est}}[k])^T \, \mathbf{Q} (x[k] - x_{\text{est}}[k]) + u^T[k] \mathbf{R} u[k] \Big) \tag{6}$$

$$x_{\text{est}} = \mathbf{L} y_{\text{est}} \tag{7}$$

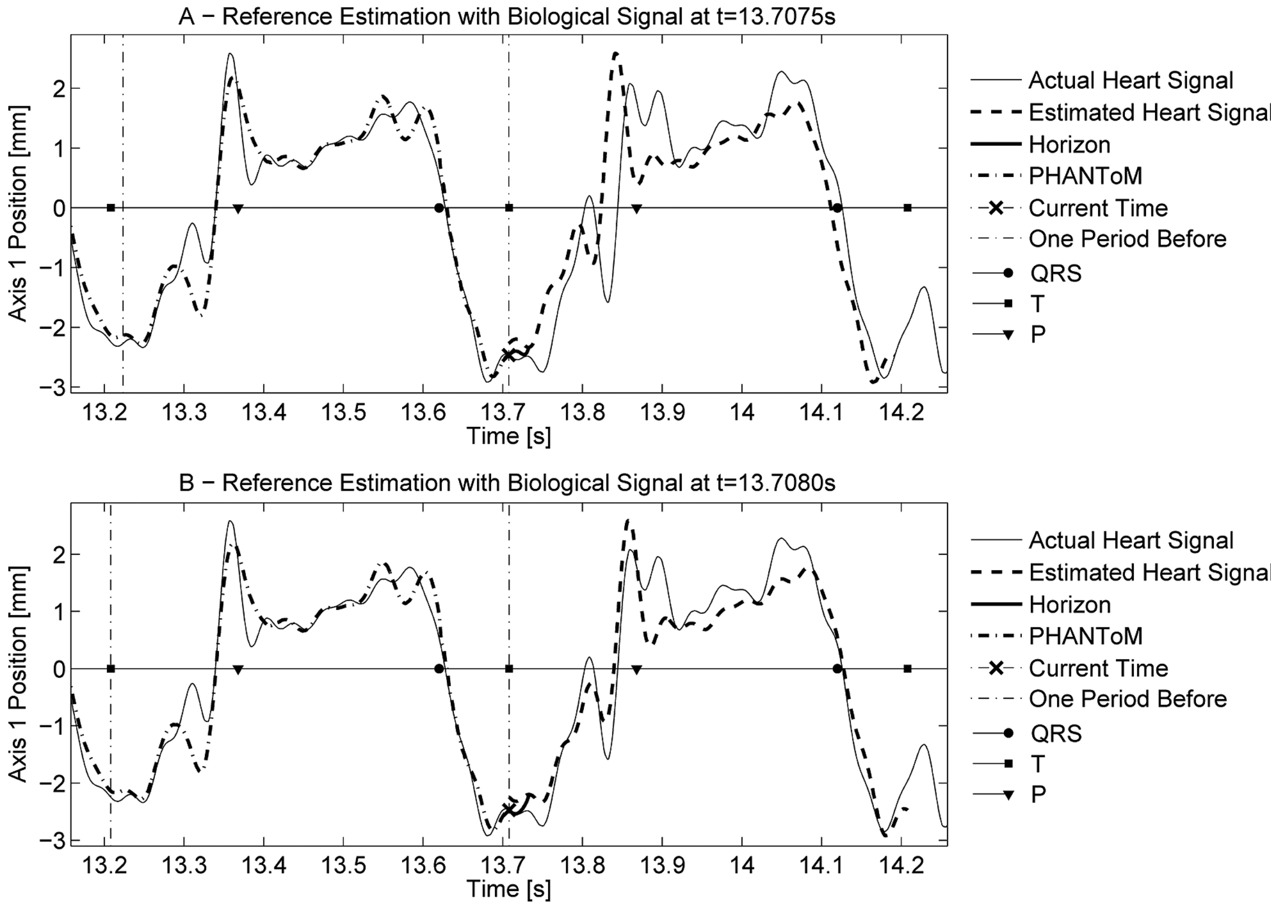

Fig. 12. Reference estimation with biological signal. (A) *Just before T wave was detected:* Estimated heart signal did not fit well with the actual heart signal. T wave detection was shown with ■ markers. (B) *T wave has been detected:* Heart period and estimated signal were adjusted. Observe that the beginning of the previous heartbeat period marker [$\cdot - \cdot - \cdot$]($t \approx 13.22$ s) was shifted back in time ($t \approx 13.21$ s) as a result of the increase in the heartbeat period. Accordingly, estimated heart signal was changed to adjust with the new period. RMS estimation error was decreased from 0.887 to 0.456 mm with the shift.

where $\mathbf{Q}$ is a non-negative definite symmetric matrix and $\mathbf{R}$ is a positive definite symmetric matrix, and $\mathbf{L}$ and $\mathbf{Q}$ are

$$\mathbf{L} = \mathbf{H}^T(\mathbf{H}\mathbf{H}^T)^{-1} \tag{8}$$

$$\mathbf{Q} = (\mathbf{I} - \mathbf{L}\mathbf{H})^T \mathbf{Q}_1 (\mathbf{I} - \mathbf{L}\mathbf{H}) + \mathbf{H}^T \mathbf{Q}_2 \mathbf{H} \tag{9}$$

where $\mathbf{Q_1}$ and $\mathbf{Q_2}$ are non-negative definite symmetric matrices.

The solution to this problem was derived using the method given in [34], and the control is

$$u[k] = -\left(\mathbf{\Gamma}^T \mathbf{S}[k+1]\mathbf{\Gamma} + \mathbf{R}\right)^{-1} \mathbf{\Gamma}^T (\mathbf{S}[k+1]\mathbf{\Phi} x[k] + \mathbf{M}[k+1]) \tag{10}$$

where $\mathbf{S}$ and $\mathbf{M}$ are given by the iterative equations

$$\begin{aligned} \mathbf{S}[k] = \mathbf{\Phi}^T(&\mathbf{S}[k+1] \\ &- \mathbf{S}[k+1]\mathbf{\Gamma}(\mathbf{\Gamma}^T\mathbf{S}[k+1]\mathbf{\Gamma} \\ &+ \mathbf{R})^{-1}\mathbf{\Gamma}^T\mathbf{S}[k+1])\mathbf{\Phi} + \mathbf{Q} \end{aligned} \tag{11}$$

$$\mathbf{M}[k] = \left(\mathbf{\Phi}^T + \mathbf{K}^T[k]\mathbf{\Gamma}^T\right)\mathbf{M}[k+1] - \mathbf{Q}\mathbf{L}y_{\mathrm{est}}[k] \tag{12}$$

and $\mathbf{K}$ is

$$\mathbf{K}[k] = -\left(\mathbf{\Gamma}^T \mathbf{S}[k+1]\mathbf{\Gamma} + \mathbf{R}\right)^{-1} \mathbf{\Gamma}^T \mathbf{S}[k+1]\mathbf{\Phi}. \tag{13}$$

The resulting control algorithm is composed of feedback and feedforward parts which are identified, respectively, as follows:

$$u_{\mathrm{fb}}[k] = -\left(\mathbf{\Gamma}^T \mathbf{S}[k+1]\mathbf{\Gamma} + \mathbf{R}\right)^{-1} \mathbf{\Gamma}^T \mathbf{S}[k+1]\mathbf{\Phi} x[k] \tag{14}$$

$$u_{\mathrm{ff}}[k] = -\left(\mathbf{\Gamma}^T \mathbf{S}[k+1]\mathbf{\Gamma} + \mathbf{R}\right)^{-1} \mathbf{\Gamma}^T \mathbf{M}[k+1] \tag{15}$$

such that

$$u[k] = u_{\mathrm{fb}}[k] + u_{\mathrm{ff}}[k]. \tag{16}$$

Parameters $\mathbf{S}$ and $\mathbf{M}$ are calculated iteratively backwards with final conditions $\mathbf{S}[T] = \mathbf{Q}$ and $\mathbf{M}[T] = 0$. The iterations are carried out for *horizon*, T, times. Every iteration corresponds to one control cycle set of gains. In effect, calculating T iterations is like calculating time varying gains up to T steps ahead even though only the gain for the current time is used. This type of control is also known as receding horizon control [34], and in this framework, we call the control defined in (10) as the receding horizon model predictive control (RHMPC). With every new control cycle, a new point on the desired signal is used and an old point is dropped in the gain calculation. The calculation is then repeated at every control cycle. The prediction horizon recedes as time progresses such that the furthermost point ahead of the horizon is considered to be moving one step for every control cycle.

V. Simulation and Experimental Results

Simulations and experiments were carried out for the estimation algorithms with Receding horizon model predictive controllers as presented in the previous section.

In order to find a baseline performance of the estimation algorithms, a RHMPC with known future reference signal was also tested. Knowing the future reference signal for the RHMPC algorithm is close to perfect tracking. However, using the future reference signal in heart tracking is not feasible as this makes the algorithm acasual. In this case, it was used to show the base line performance.

The horizon value, T, is one of the parameters that can be used to tune the algorithm. Even though tuned intuitively, the horizon does make a difference in the results whenever altered. A longer horizon generally results in more accuracy of the feedforward term, primarily because of greater foresight into the future and more iterations to calculate gains. As the horizon increases the tracking error decays exponentially. On the other hand, parameter calculations take longer. Therefore, a horizon must be chosen such that the gains can be iteratively calculated within one cycle of the control loop.

This RHMPC can handle time-varying systems and weighting matrices. For the applications used herein, constant weighting matrices, $\mathbf{Q}_1, \mathbf{Q}_2$, and $\mathbf{R}$, and a constant horizon value, T, were used along with constant state-space models. The only true time-varying gain matrix within the algorithm was $\mathbf{M}$, which was calculated from the heartbeat data. As a result, feedforward control term (15) was time-varying, and $\mathbf{M}$ was calculated iteratively on the fly every control cycle.

Feedback term (14) was not dependent on any time-varying values. Consequently, calculated gains were constant for a given horizon. Once the horizon value was set, there was no need to calculate the feedback gains in every control cycle.

Another parameter that can be used to tune the algorithm is *the error correction function order*, p of (2). p plays a good role in the performance of the algorithm along with the *horizon value*, T. For the optimum error/performance ratio, a sixth-order polynomial error correction function and a horizon value of 50 were selected.

Although using past heart cycle as estimate of future reference signals would cause large errors in extended estimates, it was not a deterministic issue in this approach, since the horizon used in the RHMPC algorithm (25 ms) was relatively short compared to the heartbeat period ($\approx$500 ms).

The robot was made to follow the combined motion of heartbeat and breathing as described in Section III. Separating the respiratory motion enabled better heart motion estimation. In terms of control performance, controlling the respiratory motion separately did not affect the heart tracking accuracy when we compared the results of the combined motion tracking with the pure heartbeat motion tracking results. This validates our earlier observation that heartbeat motion tracking will be the bottleneck in motion tracking and the breathing motion can be easily tracked using a pure feedback controller.

A. Test Bed System

In order to develop and test the algorithms, a hardware test bed system, PHANToM Premium 1.5A, was used and modeled. In modeling, experimental transfer function models for the three principle axes were determined. The specific models used and the details of the modeling methodology, and the mechanical properties of the manipulator (i.e., zero configuration, degrees of freedom) can be found in [36]. Also, the friction forces acting on the joints were modeled experimentally according to a Coulomb friction model.

The dynamic equation of the PHANToM is in the form

$$\mathbf{M}(\theta)\ddot{\theta} + \mathbf{C}(\dot{\theta}, \theta)\dot{\theta} + \mathbf{N}(\theta) = \tau \tag{17}$$

where $\theta = [\theta_1\, \theta_2\, \theta_3]^T \in \mathbb{R}^3, \mathbf{M}$ is the inertia matrix, $\mathbf{C}$ is the Coriolis matrix of the manipulator, $\mathbf{N}$ includes the gravitational and other forces—such as friction—that acts on the joints, and τ is the vector of actuator torques. The nonlinearities of the system were overcome by adding the torque that was required against the gravitational effects, $\mathbf{N}$, and Coriolis and centrifugal forces, $\mathbf{C}(\dot{\theta}, \theta)\dot{\theta}$ according to the derived dynamics. The added $\mathbf{C}(\dot{\theta}, \theta)\dot{\theta}$ term was considerably smaller than the applied torque, which is due to the quadratic dependence of this term on the joint velocities.

The PHANToM robot possesses characteristics similar to the actual surgical robot we are designing. Its lightweight links, low inertia design and low friction actuation system allows sufficient motion and speed abilities for tracking the heartbeat signal. In the experimental setup, the control algorithms were executed on a 2.6-MHz Intel Pentium 4 PC running MATLAB xPC Target v2.8 real-time kernel with a sampling time of 0.5 ms. PHANToM Premium does not come with a built-in homing option. In order to improve the accuracy of the experiments, before every experiment, the robot was brought to a selected home position, in this case the zero configuration of the manipulator, where the tracking was started. In the experiments, prerecorded heart motion signal and ECG signal were used. Raw heart position and ECG data were resampled from 257 Hz to 2 kHz by cubic interpolation, in order to use them in the control algorithms and experiments with PHANToM.

B. Experimental Results

In both simulations and experiments, the same methods and reference data were used. Some slight differences in parameters were observed due to the mathematical modeling of the robot. To validate the algorithms effectiveness, first 10 s of the 56-s data was used to tune the control parameters. Then the experiments were carried out using the 56-s-long heart data.

Matrix weighting parameters of the optimal index were tuned to minimize RMS tracking error. Parameters were selected in order to accentuate the states and, hence, regulate more quickly, with higher control efforts. Tuning was performed to avoid the high frequency resonances so that no vibration would be reflected to the structure.

For each case, experiments on PHANToM robot were repeated ten times. It was noted that the deviation between the trials are very small. Among these results, the maximum values for the *end-effector RMS and maximum position errors* in 3-D

TABLE I

END-EFFECTOR SIMULATION AND EXPERIMENTAL RESULTS: SUMMARY OF THE END-EFFECTOR RMS POSITION ERROR, MAX POSITION ERROR (IN PARENTHESIS), AND RMS CONTROL EFFORT VALUES FOR THE CONTROL ALGORITHMS USED WITH 10- AND 56-S DATA. SOME OF THE EXPERIMENTAL RESULTS ARE UNDERLINED TO POINT OUT THE EFFECT OF BIOLOGICAL SIGNAL ON THE ESTIMATION. THERE WAS A NOTICEABLE IMPROVEMENT WITH 56-S DATA BECAUSE THE HEARTBEAT PERIOD CHANGE WAS LARGER IN THE FIRST 10-S SEGMENT OF THE DATA

End-effector Tracking Results	RMS Position Error [mm] (Max Position Error) [mm]				RMS Control Effort [mNm]			
	10 s		56 s		10 s		56 s	
	Simulation	PHANToM	Simulation	PHANToM	Simulation	PHANToM	Simulation	PHANToM
Receding Horizon MPC with Exact Reference Information	0.302 (1.539)	0.284 (1.945)	0.295 (1.732)	0.277 (2.066)	14.4	48.6	14.8	46.9
Receding Horizon MPC with Reference Signal Estimation	0.718 (2.828)	0.909 (4.394)	0.726 (3.826)	0.906 (5.958)	18.5	74.8	17.6	66.5
Receding Horizon MPC with Reference Signal Estimation using ECG Signal	0.524 (2.761)	0.669 (4.308)	0.533 (3.066)	0.682 (4.921)	16.5	56.9	16.3	55.9

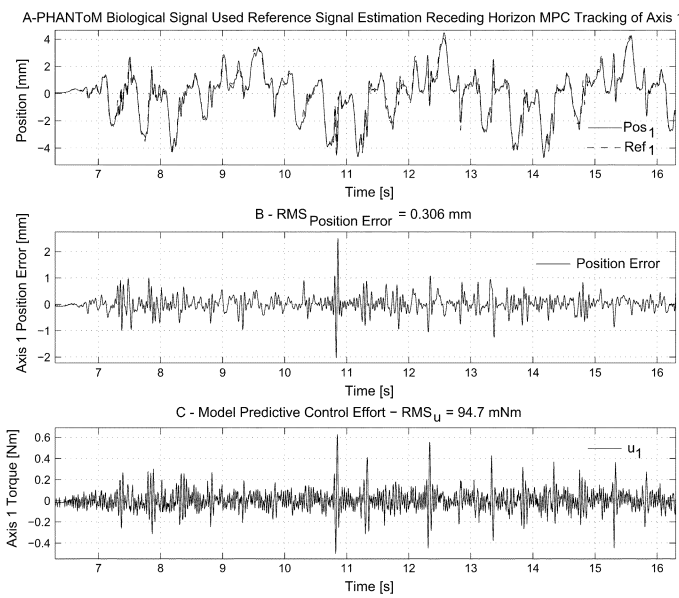

Fig. 13. PHANToM first axis results for receding horizon MPC with reference estimation using ECG signal. (A) Reference and position signals of axis 1. (B) Position error, $\mathrm{RMS}_{\mathrm{position\ error}} = 0.306$ mm. (C) Model predictive control effort signal, $\mathrm{RMS}_{\mathrm{u}} = 94.7$ mNm.

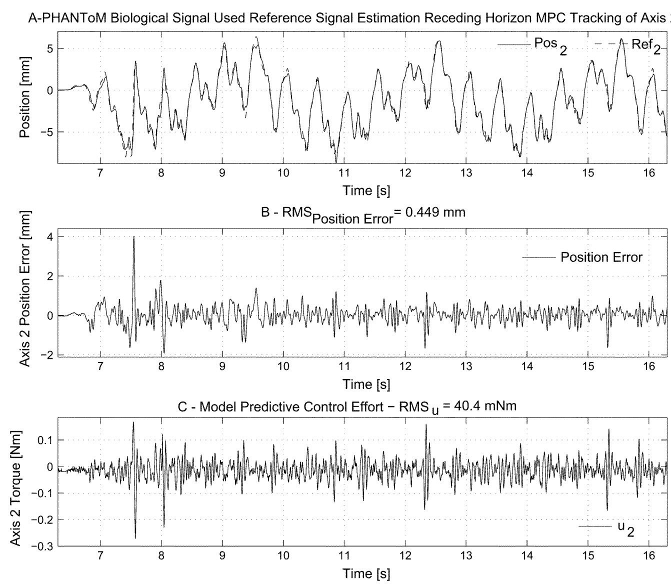

Fig. 14. PHANToM second axis results for receding horizon MPC with reference estimation using ECG Signal. (A) Reference and position signals of axis 2. (B) Position error, $\mathrm{RMS}_{\mathrm{position\ error}} = 0.449$ mm. (C) Model predictive control effort signal, $\mathrm{RMS}_{\mathrm{u}} = 40.4$ mNm.

and *RMS control efforts* are summarized in Table I to project the worst cases.

Results of the receding horizon model predictive control with reference signal estimation using ECG signal for each axis are shown in Figs. 13–15. Low-frequency respiratory motion is noticeable at the Figs. 13(A), 14(A), and 15(A). All three axes of the PHANToM demonstrated similar performance. We believe that, the maximum error values are affected from the noise in the data collected by sonomicrometric sensor. Although high-frequency parts of the raw data were filtered out, relatively low “high frequency” components stayed intact. It is unlikely that the POI on the heart is capable of moving 5 mm in a few milliseconds. The measured data has velocity peaks that are over 13 times faster than the maximum LAD velocity measurements reported in [37]. Heavy filtering should have been performed to delete the high frequency motions, but they were kept as currently we do not have an independent set of sensor measurement (such as from a vision sensor) that would validate this conjecture. This also gives a conservative measurement of the performance of the system.

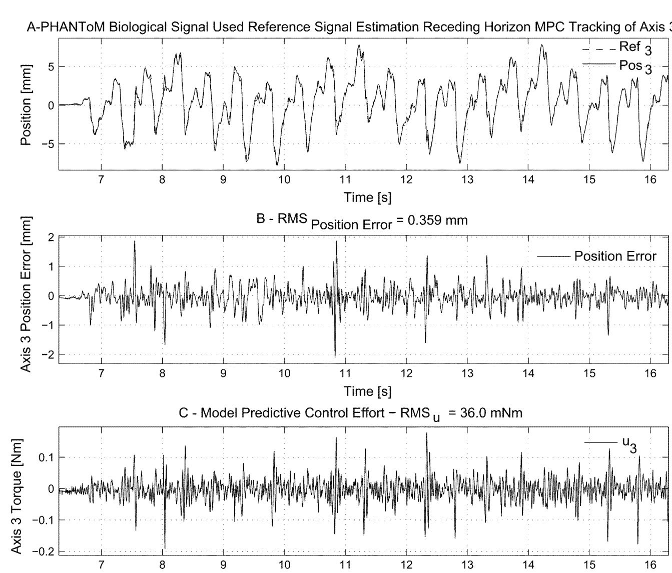

Fig. 15. PHANToM third axis results for receding horizon MPC with reference estimation using ECG signal. (A) Reference and positions signals of axis 3. (B) Position error, $\mathrm{RMS}_{\mathrm{position\ error}} = 0.359$ mm. (C) Model predictive control effort signal, $\mathrm{RMS}_{\mathrm{u}} = 36.0$ mNm.

C. Discussion of the Results

The parameters were tuned using the first 10 s of the data and validated with the 56-s data. There was less improvement in the RMS error when the 56-s data was used (see the underlined elements in Table I). This is because the heartbeat period variability was larger in the first 10-s segment of the data. The mean of the heartbeat period change was 9.3 μs for the first 10-s segment of the data and 1.6 μs for the overall data. As a result, the effect of the biological signal on the signal estimation, therefore, on the tracking error, was more pronounced in the first 10 s of the data.

If we compare the results of the algorithms with each other, as expected, the RHMPC with reference signal estimation using biological signals algorithm outperformed the RHMPC with the reference signal estimation algorithm. Results proved that by using ECG signal in the motion estimation, heart position tracking was not only improved but also became more robust. The system was more responsive to sudden changes in the heart motion with the addition of ECG signal, accordingly the variance of the error distribution decreased by half. One way ANOVA was used to test statistical significance of the results and they were found to be significantly different $(F(1,38) = 6809, p < 0.001)$. These tracking results are 2.5 times better than the best results reported in the literature [16]. Comparing the results of the predictive algorithms with the baseline performance results shows that, there is still room for improving the estimation algorithm. It is important to note that the results also need to be validated *in vivo*, which was the case in [16].

VI. Discussion

In this paper, the use of biological signals in the model-based intelligent ARMC algorithm to achieve better motion canceling was presented. The tracking problem was reduced to a reference signal estimation problem with the help of a model predictive controller. The estimated signal was created by using the last heartbeat cycle with cancelation of the position offset. Due to the quasiperiodic nature of the heart motion, heartbeat period could change in time. In order to reduce the error resulting from heart rate variations, ECG wave forms were detected and used to adjust heartbeat period during the tracking. Experimental results showed that using ECG signal in ARMC algorithm improved the reference signal estimation. It is important to note that, for patients with severe rhythm abnormalities, the detection of the ECG waveforms would present a challenge for the proposed method.

Biological signals other than ECG that can be used to assist the tracking of heart motion include aortic, atrial and ventricular blood pressures. Similar to the ECG signal, these blood pressures are significant indicatives of the heart motion as they can be used to predict when the heart valves will be opening and closing, which in turn helps us determine the distinct phases of the heart cycle. These distinct phases correspond to qualitatively different mechanical properties of the heart tissue, changing the local deformation model. The blood pressure signals also give additional independent information, which can be used in conjunction with ECG signal to improve noise robustness and to reliably detect unexpected rhythm abnormalities and arrhythmias, which will be a challenging part for the realization of the ARMC algorithm.

Image stabilization in addition to tracking the heart motion with the surgical tools is an important requirement for successful performance of off-pump bypass surgery without passive stabilization. The developed ARMC algorithm can be to be applied to camera control to achieve image stabilization.

In this study, the controller parameters were selected empirically. To the best of our knowledge, automatic selection of these parameters is still an open problem in the control literature. Although the weighting parameters were well tuned to minimize RMS error, a more comprehensive study can be conducted to automate the process and find the optimum gains.

Acknowledgment

The authors would like to thank Dr. M. Ratcliffe for his help during collection of the experimental data.

References

[1] M. F. Newman, J. L. Kirchner, B. Phillips-Bute, V. Gaver, H. Grocott, and R. H. Jones, "Longitudinal assessment of neurocognitive function after coronary-artery bypass surgery," *New England J. Med.*, vol. 344, no. 6, pp. 395–402, Feb. 2001.

[2] J. D. Puskas, C. E. Wright, R. S. Ronson, W. M. Brown, J. P. Gott, and R. A. Guyton, "Off-pump multi-vessel coronary bypass via sternotomy is safe and effective," *Ann. Thoracic Surg.*, vol. 66, no. 3, pp. 1068–1072, Sep. 1998.

[3] M. B. Ratcliffe, M.D., Chief of Surgery, San Francisco VA Medical Center, Professor in Residence. Personal Communication.

[4] V. Falk, "Manual control and tracking-A human factor analysis relevant for beating heart surgery," *Ann. Thoracic Surg.*, vol. 74, pp. 624–628, 2002.

[5] K. Sharma, W. Newman, M. Weinhous, G. Glosser, and R. Macklis, "Experimental evaluation of a robotic image-directed radiation therapy system," in *Proc. IEEE Int. Conf. Robot. Autom.*, 2000, vol. 3, pp. 2913–2918.

[6] A. Schweikard, G. Glosser, M. Bodduluri, M. Murphy, and J. Adler, "Robotic motion compensation for respiratory movement during radiosurgery," *Comput. Aided Surg.*, vol. 5, no. 4, pp. 263–277, 2000.

[7] C. Riviere, A. Thakral, I. I. Iordachita, G. Mitroi, and D. Stoianovici, "Predicting respiratory motion for active canceling during percutaneous needle insertion," in *Proc. 23rd Annu. Int. Conf. IEEE Eng. Med. Biol. Soc.*, Oct. 2001, pp. 3477–3480.

[8] A. Trejos, S. Salcudean, F. Sassani, and S. Lichtenstein, "On the feasibility of a moving support for surgery on the beating heart," in *Proc. Med. Image Comput. Comput.-Assisted Interventions*, 1999, pp. 1088–1097.

[9] A. J. Madhani, G. Niemeyer, and J. K. Salisbury, "The black falcon: A teleoperated surgical instrument for minimally invasive surgery," in *Proc. IEEE/RSJ Int. Conf. Intell. Robots Syst.*, 1998, vol. 2, pp. 936–944.

[10] Y. Nakamura, K. Kishi, and H. Kawakami, "Heartbeat synchronization for robotic cardiac surgery," in *Proc. IEEE Int. Conf. Robot. Autom.*, 2001, vol. 2, pp. 2014–2019.

[11] A. Thakral, J. Wallace, D. Tomlin, N. Seth, and N. V. Thakor, "Surgical motion adaptive robotic technology (S.M.A.R.T.): Taking the motion out of physiological motion," in *Proc. 4th Int. Conf. Med. Image Comput. Comput.-Assisted Intervention*, Oct. 2001, pp. 317–325.

[12] M. Groeger, T. Ortmaier, W. Sepp, and G. Hirzinger, "Tracking local motion on the beating heart," in *Proc. SPIE Med. Imaging Conf.*, San Diego, CA, Feb. 2002, vol. 4681, pp. 233–241.

[13] M. L. Koransky, M. L. Tavana, A. Yamaguchi, and R. Robbins, "Quantification of mechanical stabilization for the performance of offpump coronary artery surgery," presented at the Meeting Int. Soc. Minimally Invasive Cardiac Surg., 2001.

[14] T. Ortmaier, "Motion compensation in minimally invasive robotic surgery," Ph.D. dissertation, Tech. Univ. Munich, Munich, Germany, Apr. 2003.

[15] T. Ortmaier, M. Groeger, D. H. Boehm, V. Falk, and G. Hirzinger, "Motion estimation in beating heart surgery," *IEEE Trans. Biomed. Eng.*, vol. 52, no. 10, pp. 1729–1740, Oct. 2005.

[16] R. Ginhoux, J. A. Gangloff, M. F. DeMathelin, L. Soler, J. Leroy, M. M. A. Sanchez, and J. Marescaux, "Active filtering of physiological motion in robotized surgery using predictive control," *IEEE Trans. Robot.*, vol. 21, no. 1, pp. 67–79, Feb. 2005.

[17] J. Rotella, "Predictive tracking of quasi periodic signals for active relative motion cancellation in robotic assisted coronary artery bypass graft surgery," M.S. thesis, Case Western Reserve Univ., Cleveland, OH, Aug. 2004.

[18] L. Cuvillon, J. Gangloff, M. DeMathelin, and A. Forgione, "Toward robotized beating heart TECABG: Assessment of the heart dynamics using high-speed vision," in *Proc. Med. Image Comput. Comput.-Assisted Intervention*, Palm Springs, CA, Oct. 2005, vol. 2, pp. 551–558.

[19] M. B. Ratcliffe, K. B. Gupta, J. T. Streicher, E. B. Savage, D. K. Bogen, and J. L. H. Edmunds, "Use of sonomicrometry and multidimensional scaling to determine the three-dimensional coordinates of multiple cardiac locations: Feasibility and initial implementation," *IEEE Trans. Biomed. Eng.*, vol. 42, no. 6, pp. 587–598, Jun. 1995.

[20] *Digital Ultrasonic Measurement System Hardware Manual*, 6th ed. London, ON, Canada: Sonometrics.

[21] G. Kalogeros, Sonometrics, Inc., London, ON, Canada. Personal Communication.

[22] *American Heart Association*, 2006 [Online]. Available: http://www.americanheart.org

[23] J. Malmivuo and R. Plonsey, *Bioelectromagnetism—Principles and Applications of Bioelectric and Biomagnetic Fields*. Oxford, U.K.: Oxford Univ. Press, 1995.

[24] R. M. Berne and M. N. Levy, *Cardiovascular Physiology*, 8th ed. St. Louis, MO: Mosby, 2001.

[25] R. M. Berne and M. N. Levy, *Principles of Physiology*, 3rd ed. St. Louis, MO: Mosby, 2000.

[26] R. Poli, S. Cagnoni, and G. Valli, "Generic design of optimum linear and nonlinear QRS detection," *IEEE Trans. Biomed. Eng.*, vol. 42, no. 11, pp. 1137–1141, Nov. 1995.

[27] V. X. Afonso, W. J. Tompkins, T. Q. Nguyen, and S. Luo, "ECG beat detection using filter banks," *IEEE Trans. Biomed. Eng.*, vol. 46, no. 2, pp. 192–201, Feb. 1999.

[28] I. Dotsinsky and T. Stoyanov, "Ventricular beat detection in single channel electrocardiograms," *BioMed. Eng. OnLine*, vol. 3, no. 3, 2004.

[29] C. Li, C. Zheng, and C. Tai, "Detection of ECG characteristic points using wavelet transforms," *IEEE Trans. Biomed. Eng.*, vol. 42, no. 1, pp. 21–28, Jan. 1995.

[30] I. Chirstov, "Real time electrocardiogram QRS detection using combined adaptive threshold," *BioMed. Eng. OnLine*, vol. 3, no. 28, 2004.

[31] M. Bahoura, M. Hassani, and M. Hubin, "DSP implementation of wavelet transform for real wave forms detection and heart rate analysis," *Comput. Meth. Programs Biomed.*, vol. 52, pp. 35–44, 1997.

[32] *MIT-BIH Arrhythmia Database*, PhysioNet, 1980 [Online]. Available: http://www.physionet.org/physiobank/database/mitdb/

[33] C. E. Garcia, D. M. Prett, and M. Morari, "Model predictive control: Theory and practice—A survey," *Automatica*, vol. 25, no. 3, pp. 335–348, 1989.

[34] E. Camacho and C. Bordons, *Model Predictive Control*. New York: Springer, 1999.

[35] B. D. Anderson and J. B. Moore, *Optimal Control Linear Quadratic Methods*. Englewood Cliffs, NJ: Prentice-Hall, 1990.

[36] M. C. Çavuşoğlu, D. Feygin, and F. Tendik, "A critical study of the mechanical and electrical properties of the PHANToM haptic interface and improvement for high performance control," *Presence*, vol. 11, no. 6, pp. 555–568, 2002.

[37] G. Shechter, J. R. Resar, and E. R. McVeigh, "Displacement and velocity of the coronary arteries: Cardiac and respiratory motion," *IEEE Trans. Med. Imag.*, vol. 25, no. 3, pp. 369–375, Mar. 2006.

Özkan Bebek (S'06) received the B.S. degree in mechanical engineering from the Middle East Technical University, Ankara, Turkey, in 2001, and the M.S. degree in mechatronics from Sabanci University, Istanbul, Turkey, in 2003. He is currently working toward the Ph.D. degree in the Electrical Engineering and Computer Science Department, Case Western Reserve University, Cleveland, OH.

His research interests include medical robotics, mechatronics, and control systems.

M. Cenk Çavuşoğlu (SM'93–M'01–SM'06) received the B.S. degree in electrical and electronic engineering from the Middle East Technical University, Ankara, Turkey, in 1995, and the M.S. and Ph.D. degrees in electrical engineering and computer sciences from the University of California (UC), Berkeley, in 1997 and 2000, respectively.

He was a Postdoctoral Researcher and Lecturer at the Department of Electrical Engineering and Computer Sciences, UC Berkeley, from 2000 to 2002. He is now an Assistant Professor of Electrical Engineering and Computer Science at Case Western Reserve University, Cleveland, OH. His research interests include robotics (medical robotics and haptics), virtual environments and computer graphics (surgical simulation and physical modeling), and systems and control theory.

Dr. Çavuşoğlu is an Associate Editor of the IEEE TRANSACTIONS ON ROBOTICS.